The Astrophysical Journal, 861:130 (8pp), 2018 July 10 https://doi.org/10.3847/1538-4357/aac77c

High-redshift BL Lac Objects: Spectroscopy of Candidates

M. Landoni[1], S. Paiano[2,3], R. Falomo[2], R. Scarpa[4], and A. Treves[5]
[1] INAF, Osservatorio Astronomico di Brera, Via E. Bianchi 46 I-23807 Merate (LC), Italy
[2] INAF, Osservatorio Astronomico di Padova, Vicolo dell'Osservatorio 5 I-35122 Padova (PD), Italy
[3] Università di Padova and INFN, Via Marzolo 8, I-35131 Padova, Italy
[4] Instituto de Astrofisica de Canarias, C/O Via Lactea, s/n E38205, La Laguna (Tenerife), Espana
[5] Università degli Studi dell'Insubria, Via Valleggio 11 I-22100 Como, Italy
Received 2017 December 29; revised 2018 May 8; accepted 2018 May 9; published 2018 July 12

Abstract

We report on 16 BL Lacertae objects that were proposed to be at $z > 1$. We present spectroscopic observations secured at the 10.4 m GTC that allowed us to assess the redshift of these sources. In particular, for five objects, we disprove the previous value of the redshift reported in the literature and found that they lie at $z < 1$. Moreover, two of them exhibit broad emission lines that are not characteristic of BL Lacertae objects. On the other hand, for eight targets, we improve the tentative value of z, previously based on only one feature, by detecting a number of emission lines. Finally, in three cases, we detect the onset of the Lyα forest at $z > 2.50$. Based on the new high quality spectra, we found that only half of the observed objects can be classified as bona-fide BL Lacs.

Key words: BL Lacertae objects: general – galaxies: high-redshift

Supporting material: figure set, machine-readable tables

1. Introduction

BL Lac objects (BLLs) are active galactic nuclei that show a strong, luminous continuum that arises from nonthermal emission and are characterized by variability at all wavelengths, from near-IR to γ-rays (see, e.g., Falomo et al. 2014; Madejski & Sikora 2016). These properties are explained assuming the presence of a relativistic jet pointed in the direction of the observer. BLLs, which dominate the extragalactic γ-rays sky, are a unique laboratory for high energy astrophysics and fundamental physics. However the determination of their distance, which is crucial to fully understand their physical properties, is a challenging task. In fact, their optical spectrum is quasi-featureless and the nonthermal continuum outshines both the superposed thermal contribution due to the stellar component of the host galaxy and the emission lines generated by fluorescence in clouds surrounding the central black hole, thus preventing a determination of the redshift. Moreover, when spectral lines are detected, they are characterized by very small (few Å) equivalent width (EW) and thus high quality optical spectra in terms of signal-to-noise ratio (S/N) and spectral resolution is required to reveal them (e.g., Sbarufatti et al. 2006; Shaw et al. 2013; Landoni et al. 2014; Pita et al. 2014; Paiano et al. 2018, 2017a, 2017b).

Up to now, only very few BLL objects have a well determined redshift at $z \gtrsim 1$. For instance, according to the latest version of the Roma BZ-Catalog (Massaro et al. 2015a, 2015b) there are ~1000 sources classified as genuine BLL objects and for about 600 targets the redshift is unknown. For the remaining 400, there is a value for the redshift (but for ~100 the z is tentative) and only 15 objects are reported at $z > 1$. Remarkably, for 12 of them, the value of z is also uncertain. The discovery of a number of BLL objects at $z \gtrsim 1$ is fundamental to assess their luminosity function and cosmic evolution, particularly to clarify if it is positive or negative (e.g., Ajello et al. 2014 and references therein). Moreover, when detected at very high energy with Cherenkov Telescopes, BLLs at $z \gtrsim 1$ are precious probes to constrain the extragalactic background light (e.g., Franceschini & Rodighiero 2017) and also to test some exotic effects coming from nonstandard physics, like Lorentz-invariance violation (e.g., Tavecchio & Bonnoli 2016) or to indirectly detect axion like particles (e.g., de Angelis et al. 2011).

Here we focus on a sample of BLLs proposed to be at $z > 1$ and selected from the Sloan Digital Sky Survey (SDSS), Section 2.

The paper is organized as follows: We give details on sample selection and data reduction in Section 2, while we present our main results in Section 3. Notes on individual observed sources are reported in Section 4, and we draw our conclusions in Section 5. Throughout the paper, we adopt the following cosmological parameters: $H_0 = 70\,\mathrm{km\,s^{-1}\,Mpc^{-1}}$, $\Omega_\Lambda = 0.7$, and $\Omega_m = 0.3$.

2. Sample, Reduction, and Data Analysis

We selected targets that are candidates for being at high redshift ($z \gtrsim 1$) from the list of BLL sources, based on SDSS Data Release 7 spectra provided by Plotkin et al. (2010; see Table 4 in their paper). This data set includes 637 objects and only half of them (367) have redshift. Of the latter, only 28 posses indications that $z > 1$ and, for 18, the measurement is also uncertain. We have undertaken a spectroscopic study of these targets using high S/N spectra secured at large telescopes. From the initial database, we excluded objects with apparent magnitudes $\gtrsim$20, yielding a sample of 24 sources. In this paper, we present 16 objects observed with Gran Telescopio CANARIAS (GTC) equipped with OSIRIS. Details are reported in Table 1.

The observations were obtained in service mode at the GTC using the low resolution spectrograph OSIRIS (Cepa et al. 2003). The instrument was configured with the grisms R1000B and R1000R,[6] in order to cover the whole spectral range of 4100–9500 Å, and with a slit width = 1″ yielding a spectral resolution $\lambda/\Delta\lambda = 800$.

[6] http://www.gtc.iac.es/instruments/osiris/osiris.php

Table 1
The Sample of High-redshift SDSS BL Lac Candidates

Object Name	R.A. (J2000)	δ (J2000)	l	b	V	$E(B-V)$[a]	Redshift[b]	Redshift Type
SDSS J072659.52+373423.0	07:26:59.52	+37:34:23.0	181.06	22.77	19.38	0.050	1.577	T
SDSS J090818.95+214820.0	09:08:18.95	+21:48:20.0	206.06	39.35	19.24	0.031	2.089	T
SDSS J092902.42+194525.1	09:29:02.40	+19:45:25.2	210.69	43.29	19.25	0.050	1.774	T
SDSS J094257.81−004705.2	09:42:57.82	−00:47:05.3	236.68	36.82	19.00	0.045	1.360	T
SDSS J101115.63+010642.5	10:11:15.64	+01:06:42.5	240.21	43.63	19.40	0.041	1.479	T
SDSS J120059.69+400913.1	12:00:59.68	+40:09:13.1	158.44	73.30	19.90	0.200	$\geqslant$3.370	LL
SDSS J121037.35+525341.9	12:10:37.34	+52:53:41.8	136.61	63.13	18.80	0.020	0.917	T
SDSS J123132.37+013814.1	12:31:32.36	+01:38:14.0	291.50	64.06	19.20	0.015	$\geqslant$3.147	LL
SDSS J124030.93+344527.5	12:40:30.90	+34:45:27.5	139.30	82.02	19.35	0.010	1.642	T
SDSS J124700.72+442318.8	12:47:00.72	+44:23:18.8	125.59	72.71	18.90	0.020	1.812	T
SDSS J130925.52+430505.5	13:09:25.52	+43:05:05.6	111.20	73.63	17.30	0.019	1.154	T
SDSS J132802.09+112913.6	13:28:02.09	+11:29:13.7	333.48	72.15	18.53	0.025	1.827	T
SDSS J144050.14+333350.2	14:40:50.14	+33:33:50.1	54.91	65.61	18.40	0.100	1.774	T
SDSS J145059.98+520111.7[c]	14:50:59.98	+52:01:11.7	89.13	56.53	18.90	0.060	$\geqslant$2.471	LL
SDSS J152422.56+374034.1	15:24:22.56	+37:40:34.2	60.934	56.30	19.80	0.034	1.219	T
SDSS J170108.89+395443.0	17:01:08.89	+39:54:43.0	63.96	37.48	19.30	0.024	1.889	T

Notes. Column 1: name of the target. Column 2: right Ascension. Column 3: declination. Column 4: Galactic coordinate l. Column 5: Galactic coordinate b. Column 6: magnitude from catalog. Column 7: reddening (from NED). Column 8: redshift. Column 9: type of redshift: T—tentative; LL—lower limit from intervening systems.
[a] Extinction values taken from NED.
[b] Redshift from Plotkin et al. (2010). For SDSS J145059.98+520111.7 redshift is given by Liao et al. (2015).
[c] Published in Paiano et al. (2017b).

(This table is available in machine-readable form.)

For each grating, we obtained three individual exposures sequentially under the same sky condition and instrument configuration that were combined in order to perform a good cleaning of cosmic rays and CCD cosmetic defects. Wavelength calibration was performed using the spectra of Hg, Ar, Ne, and Xe lamps and provides an accuracy of 0.1 Å over the whole spectral range. For each object, the spectra obtained with the two grisms were joined into a final spectrum covering the whole spectral range. Data were corrected for atmospheric extinction using the mean La Palma site extinction table.[7] Relative flux calibration was provided by spectro-photometric standard stars secured during the same night of the target observation. Absolute flux calibration was assessed using relative photometry of objects in the Sloan r filter acquisition image. The accuracy of the calibration is about $\Delta m \sim 0.1$. We exploited for our analyses the software procedures developed for our long-term optical spectroscopy programs at large telescopes (like ESO-VLT and GTC) specifically aimed at measuring the redshifts of BLLs (Sbarufatti et al. 2006; Sandrinelli et al. 2013; Landoni et al. 2015a; Paiano et al. 2016, 2017a, 2017b). Detailed information on the observations and target magnitudes at the time of data acquisition are given in Table 2.

3. Results

We report the spectra of BLLs in Figure 1 (close-up of the faintest spectral features in Figure 2) and we provide the full figure set and machine readable data online at http://archive.oapd.inaf.it/zbllac/. We enhance spectral features by showing both the flux calibrated and the normalized spectrum that was obtained by dividing the calibrated spectrum by a power-law continuum in all cases where the spectrum could be fitted in this way (see also individual notes in Section 4). This procedure allows us to emphasize weak features that appear clearer on the normalized data.

We evaluate the S/N in a number of spectral regions (see Table 3) adopting the procedure described in Paiano et al. (2017a). The use of GTC+OSIRIS enabled us to obtain spectra with S/Ns superior to that of SDSS (about a factor of ∼2). In detail, the average S/N of GTC spectra is assessed to be ∼35, while for SDSS data it is ∼15 and no significant variabilities of the targets in terms of apparent r band magnitude have been detected. All spectra were carefully inspected to search for emission and or absorption lines. When a possible feature is found, we check its reliability by comparing the three independent exposures (see Section 2) and we consider it to be reliable if detected above the noise level in all three acquired frames.

For five objects, we disprove the value of the redshift previously reported in the literature. For one of them, SDSS J092902.42+194525.1, the spectrum appears completely featureless and we infer $z \geqslant 0.35$ from the absence of starlight from host galaxies (Sbarufatti et al. 2006; Paiano et al. 2017b), while, for the remaining sources, we give new values for the redshift. In particular, for SDSS J072659.52+373423.0, we measure $z = 0.791$ by detecting Ca II H-K lines (3934–3968 Å) from the host galaxy, while, for SDSS J101115.63+010642.5, we found at $z = 0.857$ emission features from [Ne V] (3346 Å), [O II] (3727 Å), Hβ (4861 Å), and [O III] (4959–5007 Å). In the case of SDSS J124700.72+442318.8, we confirm the presence of a feature at λ 7860 Å but the identification with Mg II (2800 Å), as suggested by Plotkin et al. (2010), is unlikely since it appears rather narrow (FWHM $\sim$ 300 km s^{-1}) and weak (EW ∼2.30 Å) and we suggest identification as [O III] (5007 Å) at $z = 0.569$. Finally, for SDSS J132802.09+112913.6, we detect emission lines from Mg II (2800 Å),

[7] https://www.ing.iac.es/Astronomy/observing/manuals/

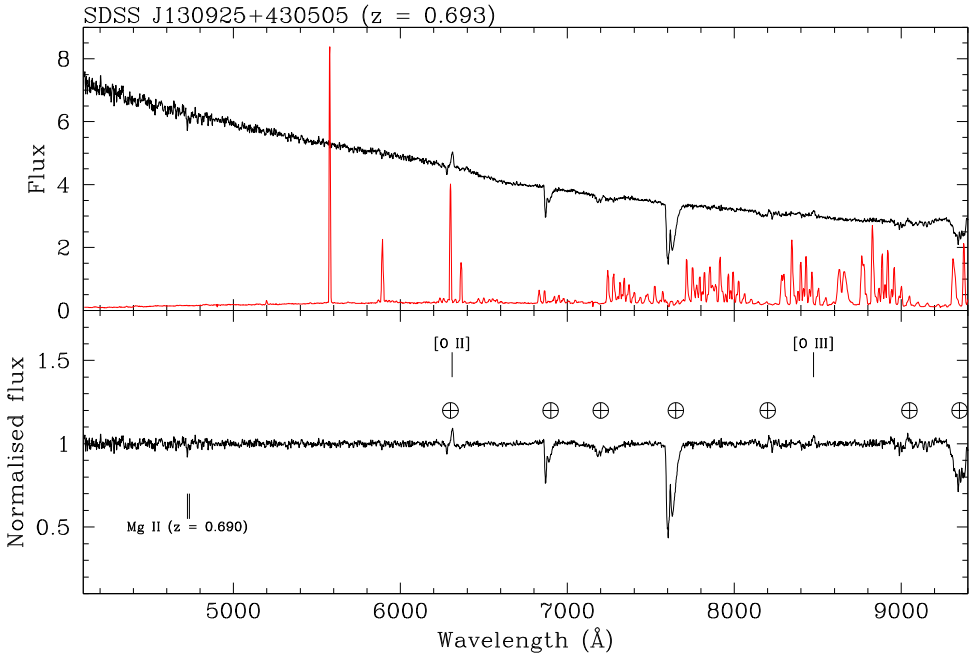

Figure 1. Sample spectrum of the high-redshift SDSS BLLs obtained at GTC. Top panel: flux calibrated and deredded spectra are in black. The red solid line is the sky spectrum in arbitrary units reported for the sake of comparison. Bottom panel: normalized spectra. The main telluric bands are indicated by ⊕. The absorption features from the interstellar medium of our galaxies are labeled as IS (Inter-Stellar). Data are available at http://www.oapd.inaf.it/zbllac/.

(The complete figure set (15 images) is available.)

Table 2
Log Observations of High-z SDSS Sources Obtained at GTC

	Grism B			Grism R			
Object	$t_{\rm Exp}$ (s)	Date	Seeing ($''$)	$t_{\rm Exp}$ (s)	Date	Seeing ($''$)	r
SDSS J072659.52+373423.0	1500	2015 Jan 29	2.2	2400	2015 Jan 29	2.1	19.80
SDSS J090818.95+214820.0	1800	2015 Jan 30	2.1	2500	2015 Jan 30	1.8	19.15
SDSS J092902.42+194525.1	1500	2015 Mar 14	2.1	2400	2015 Mar 14	1.9	19.60
SDSS J094257.81-004705.2	1250	2015 Feb 10	1.7	1800	2015 Feb 10	1.9	19.00
SDSS J101115.63+010642.5	1800	2015 Feb 11	1.5	2500	2015 Feb 11	1.4	18.90
SDSS J120059.69+400913.1	7200	2015 Feb 24	1.8	7200	2015 Feb 28	2.1	19.50
SDSS J121037.35+525341.9	900	2015 Feb 12	2.8	1800	2015 Feb 12	2.3	19.20
SDSS J123132.37+013814.1	1500	2015 Jan 30	2.0	2100	2015 Jan 30	1.8	18.80
SDSS J124030.93+344527.5	1800	2015 Feb 12	1.7	2400	2015 Feb 12	1.9	19.00
SDSS J124700.72+442318.8	1300	2015 Feb 12	2.5	1500	2015 Feb 12	2.4	19.10
SDSS J130925.52+430505.5	300	2015 Feb 04	1.0	700	2015 Feb 04	0.9	17.00
SDSS J132802.09+112913.6	600	2015 Feb 04	1.1	1500	2015 Feb 04	0.9	18.50
SDSS J144050.14+333350.2	900	2015 Feb 04	0.9	900	2015 Feb 04	0.8	18.60
SDSS J145059.98+520111.7	1500	2015 Mar 14	2.0	1800	2015 Mar 14	1.9	18.90
SDSS J152422.56+374034.1	2400	2015 Feb 25	1.2	3000	2015 Mar 14	1.8	19.40
SDSS J170108.89+395443.0	2400	2015 Mar 14	2.1	2400	2015 Mar 14	2.0	19.20

Note. Column 1: name of the target. Column 2: exposure time for R1000B grism (sec). Column 3: date of observation of grism R1000B. Column 4: seeing during acquisition of R1000B spectrum. Column 5: exposure time for R1000R grism. Column 6: date of observation of grism R1000R. Column 7: seeing during acquisition of R1000R spectrum. Column 8: magnitude measured from acquisition image in r band.

(This table is available in machine-readable form.)

[Ne V] (3346 Å), and [O II] (5007 Å) all at the same redshift, $z = 0.580$.

Regarding the remaining 11 targets, for 3 of them (namely SDSS J120059.69+400913.1, SDSS J123132.37+013814.1, and SDSS J145059.98+520111.7) a spectroscopic lower limit to z is set on the basis of detection of onset of the Lyα forest. We confirmed the literature values and we did not find any further emission lines redward of the Lyα forest, though our new GTC data present in that region an S/N that is a factor of $\sim$5 higher than SDSS spectra. For eight cases (SDSS J090818.95+214820.0, SDSS J094257.81–004705.2, SDSS J121037.35+525341.9, SDSS J124030.93+344527.5, SDSS J130925.52+430505.5, SDSS 144050.14+333350.2, SDSS J152422.56+374034.1, and SDSS J170108.89+395443.0), we endorse the proposed tentative value of the redshift that was based on only one emission line, by

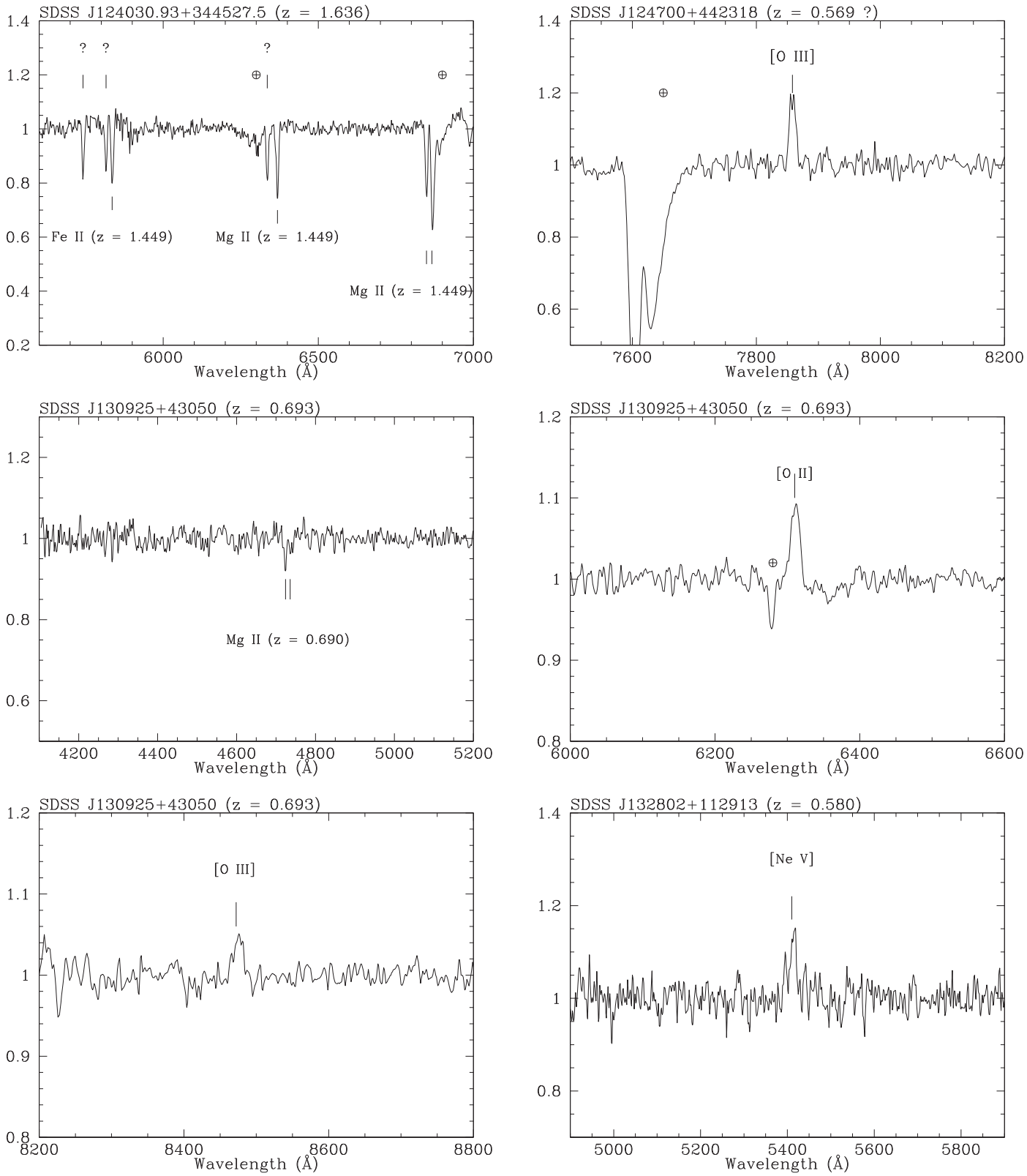

Figure 2. Close-up of the normalized spectra around the detected spectral features. Main telluric bands are indicated as ⊕, spectral lines are marked by line identification.

measuring further spectral features that enforce the values of z. We report in Table 4 all the spectral features identified in our sample and discuss each target in detail in the next section.

4. Notes for Individual Sources

SDSS J072659.52+373423.0: On the basis of the emission feature at λ7200 Å in the SDSS spectrum, Plotkin et al. (2010) suggested a tentative redshift of $z = 1.577$. We do

Table 3
Properties of the Optical Spectra of High z Sources

OBJECT	S/N GTC	EW_{min}	z	Class
SDSS J072659.52+373423.0	20	1.00–1.50	$0.791^{(g)}$	B
SDSS J090818.95+214820.0	30	0.65–1.20	2.088	B
SDSS J092902.42+194525.1	25	0.70–1.10	$\geqslant 0.35^{(ll)}$	B
SDSS J094257.81-004705.2	35	0.60–0.90	1.363	B
SDSS J101115.63+010642.5	50	0.30–0.80	0.857	Q
SDSS J120059.69+400913.1	25	0.70–1.30	$\geqslant 3.367^{(i)}$	B
SDSS J121037.35+525341.9	40	0.30–1.10	0.916	Q
SDSS J123132.37+013814.1	30	0.40–1.00	$\geqslant 3.140^{(i)}$	B
SDSS J124030.93+344527.5	50	0.37–0.80	1.636	B
SDSS J124700.72+442318.8	60	0.20–0.90	0.569 ?	B
SDSS J130925.52+430505.5	100	0.55–0.90	0.693	B
SDSS J132802.09+112913.6	30	0.55–1.00	0.580	Q
SDSS J144050.14+333350.2	30	0.50–0.90	1.747	Q
SDSS J145059.98+520111.7	70	0.50–0.90	$\geqslant 2.470^{(i)}$	B
SDSS J152422.56+374034.1	40	0.60–1.00	1.219	Q
SDSS J170108.89+395443.0	25	0.60–1.00	1.895	Q

Note. Column 1: name of the target. Column 2: average GTC S/N of the spectrum. Column 3: range of the minimum equivalent width (EW_{min}) derived from different regions of the spectrum (see Paiano et al. 2017b). Column 4: proposed redshift from this work. The superscript letters indicate g = host galaxy absorption, i = intervening absorption, ll = lower limit of the redshift by assuming a BL Lac host galaxy with $M_R = -22.9$. Column 5: class of the object (B: BLL, Q: FSRQ).
(This table is available in machine-readable form.)

not confirm the presence of this feature in our spectrum (S/N = 20); though, we detect an absorption doublet at $\lambda\lambda$7043–7107 Å that we identify as Ca II (3934–3968 Å) at $z = 0.791$. This feature, although it is encompassed by two atmospheric absorption bands, is firmly detected since it is revealed in both R1000B and R1000R spectra (see Figure 3).
SDSS J090818.95+214820.0: A redshift of $z = 2.089$ was proposed by Plotkin et al. (2010) on the basis of a weak emission line at 8600 Å ascribed to Mg II (2800 Å). We confirm the presence of this emission line at 8650 Å in our data (S/N = 30) and we also detect a broad feature at ∼4789 Å corresponding to C IV (1909 Å), therefore, firmly confirming the redshift.
SDSS J092902.42+194525.1: Plotkin et al. (2010) proposed a tentative redshift of $z = 1.774$ based on a narrow emission line at 7770 Å. We do not confirm this structure and suspect that it might be an artifact of the filtering procedure of the SDSS spectrum since it is not present in the unfiltered data. No other emission or absorption lines are detected in our spectrum (S/N = 25); therefore, the redshift remains unknown. From the minimum detectable EW_{min} of starlight features from the host galaxy (Paiano et al. 2017a), we set a lower limit to $z \geqslant 0.35$. According to the expected number of Mg II intervening systems for sources at $z > 1$, the probability of not detecting any one of them as in the case of this object is roughly 0.25, suggesting that it is unlikely that this BLL lies at high redshift.
SDSS J094257.81-004705.2: In our optical spectrum (S/N = 35), we detect two emission lines at 4509 and 6610 Å that we identify as C III] and Mg II at $z = 1.36$. This confirms the previous tentative redshift based only on one spectral feature (Plotkin et al. 2010). In addition, we also measure an intervening Mg II absorption system at $z = 0.819$.
SDSS J101115.63+010642.5: A single broad emission feature at ∼9200 Å is visible in the SDSS spectrum. It was erroneously interpreted as Lyα by the SDSS automatic procedure leading to the tentative redshift $z > 5$. In the work of Plotkin et al. (2010), the authors suggest a tentative redshift of $z = 1.479$ on the basis of the narrow feature at ∼6930 Å. In our new data (S/N = 50), we detect the two features at 6929 and 9209 Å, which we interpret as the [O II] and [O III] doublet. Moreover, other fainter emission lines due to [Ne V] and Hβ that are all consistent at a more modest redshift of $z = 0.857$ are revealed.
SDSS J120059.69+400913.1: The lower limit of redshift of the source $z \geqslant 3.37$ was derived robustly by the SDSS and confirmed in the sample of Plotkin et al. (2010) by detecting firmly the onset of the Lyα forest. Our new GTC data (S/N = 25) presents an S/N about a factor of ∼5 higher than SDSS in the region 5400–9200 Å and, apart from absorption features from intervening systems, does not present any emission line down to EW $\geqslant$ 0.70.
SDSS J121037.35+525341.9: A faint broad emission line at 5350 Å is visible in the SDSS spectrum. If identified as Mg II (2800 Å), a tentative redshift of $z = 0.916$ is derived (Plotkin et al. 2010). The newly GTC-OSIRIS data (S/N = 40) confirm the presence of the feature at the same wavelength and in addition we clearly detect the [O II] (3727 Å) emission line at λ7142 Å.
SDSS J123132.37+013814.1: The lower limit of the redshift was set $z \geqslant 3.147$ from the detection of the Lyα forest in the SDSS spectra. We confirm the detection of the Lyα forest (Plotkin et al. 2010) at the same redshift, while we do not measure any further emission line in the region 5200–9200 Å at (S/N = 30) and with EW $\geqslant \sim 0.40$ making this source, apart from line-of-sight intervening systems, intrinsically featureless.
SDSS J124030.93+344527.5: A tentative redshift of $z = 1.642$ was proposed on the basis of a marginally detected weak emission line at $\lambda \sim 7390$ Å ascribed to Mg II (see Plotkin et al. 2010). We confirm the presence of the feature and we further detect an intervening absorption system at $z = 1.449$ by measuring absorption lines from Mg II and Fe II at the same redshift. We also note the presence of narrow absorption features in the GTC spectrum

Table 4
Measurements of Spectral Lines

Object	λ_{obs} Å	EW (Observed) Å	Line ID	z_{line}	Luminosity log ($L_{\odot}$)	Type
SDSS J072659.52+373423.0	7043.80	2.60	Ca II (3934)	0.791	⋯	G
	7107.40	1.80	Ca II (3968)	0.791	⋯	G
SDSS J090818.95+214820.0	4789.20	20.10	C IV (1550)	2.088	43.45	E
	8650.40	19.30	Mg II (2800)	2.089	43.43	E
SDSS J094257.81−004705.2	4509.20	14.90	C III] (1909)	1.362	42.90	E
	5086.39	2.30	Mg II (2796)	0.819	⋯	A
	5100.18	2.10	Mg II (2803)	0.819	⋯	A
	6608.92	10.30	Mg II (2800)	1.363	42.75	E
SDSS J101115.63+010642.5	6310.00	3.50	[Ne V] (3346)	0.885*	⋯	E
	6929.00	3.00	[O II] (3727)	0.858*	⋯	E
	9028.00	2.70	Hβ (4861)	0.857*	⋯	E
	9209.00	30.00	[O III] (4959)	0.857*	⋯	E
	9298.00	50.00	[O III] (5007)	0.857*	⋯	E
SDSS J120059.69+400913.1	5310.20	56.10	Lyα (1216)	3.367	⋯	A
	5991.40	2.50	Mg II (2796)	1.142	⋯	A
	6003.20	2.00	Mg II (2803)	1.142	⋯	A
	5919.62	2.50	Fe II (2382)	1.484	⋯	A
	6459.50	2.00	Fe II (2600)	1.484	⋯	A
	6946.50	4.50	Mg II (2796)	1.484	⋯	A
	6964.10	3.00	Mg II (2803)	1.484	⋯	A
SDSS J121037.35+525341.9	5360.20	29.10	Mg II (2800)	0.917	43.60	E
	7142.40	3.70	[O II] (3727)	0.916	42.60	E
SDSS J123132.37+013814.1	5434.00	49.60	Lyα (1216)	3.140	⋯	A
	5527.20	2.00	Mg II (2796)	0.977	⋯	A
	5541.50	1.50	Mg II (2803)	0.977	⋯	A
	6154.00	3.50	Mg II (2796)	1.200	⋯	A
	6167.10	1.50	Mg II (2803)	1.200	⋯	A
	7812.20	1.50	Fe II (2600)	2.004	⋯	A
	8401.30	5.00	Mg II (2796)	2.004	⋯	A
	8422.20	3.50	Mg II (2803)	2.004	⋯	A
SDSS J124030.93+344527.5	5741.10	1.70	?	?	⋯	A
	5815.50	1.50	?	?	⋯	A
	5835.80	2.00	Fe II (2382)	1.449	⋯	A
	6335.20	2.20	?	?	⋯	A
	6368.60	5.00	Fe II (2600)	1.449	⋯	A
	6848.90	5.00	Mg II (2796)	1.449	⋯	A
	6866.30	7.00	Mg II (2803)	1.449	⋯	A
	7390.10	12.30	Mg II (2800)	1.636	43.00	E
SDSS J124700.72+442318.8	7858.20	2.30	[O III] (5007) ?	0.569 ?	41.00	E
SDSS J130925.52+430505.5	4724.55	0.40	Mg II (2796)	0.690	⋯	A
	4736.70	0.20	Mg II (2803)	0.690	⋯	A
	6309.35*	1.70	[O II] (3727)	0.693	42.00	E
	8474.30	0.50	[O III] (5007)	0.693	41.40	E
SDSS J132802.09+112913.6	4409.90	86.70	Mg II (2800)	0.577	42.90	E
	5410.40	3.50	[Ne V] (3426)	0.578	41.50	E
	7915.10	6.50	[O III] (5007)	0.580	41.80	E
SDSS J144050.14+333350.2	4254.90	15.30	C IV (1550)	1.745	43.35	E
	4414.15	1.35	Mg II (2796)	0.578	⋯	A
	4426.24	1.20	Mg II (2803)	0.579	⋯	A
	5245.80	30.35	C III] (1909)	1.747	43.70	E
	6063.04	2.20	Mg II (2803)	1.168	⋯	A
	6078.50	1.30	Mg II (2796)	1.168	⋯	A
	∼7700	18.00	Mg II (2800)	∼1.74*	⋯	E
SDSS J152422.56+374034.1	4235.40	5.30	C III] (1909)	1.218	42.10	E
	6204.50	64.30	Mg II (2800)	1.219	42.90	E

Table 4
(Continued)

Object	λ_{obs} Å	EW (Observed) Å	Line ID	z_{line}	Luminosity log ($L_{\odot}$)	Type
SDSS J170108.89+395443.0	4490.50	30.00	C IV (1550)	1.895	43.40	E
	8120.50	11.10	Mg II (2800)	1.896	42.90	E

Note. Column 1: name of the target. Column 2: barycenter of the detected line. Column 3: measured equivalent width. Column 4: line identification. Column 5: spectroscopic redshift (the $*$ indicates that the value is determined from the barycenter of detected lines contaminated by telluric absorptions). Column 6: line luminosity (only for emission features). Column 7: feature type: G—absorption from host galaxy; E—emission line; A—absorption lines.

(This table is available in machine-readable form.)

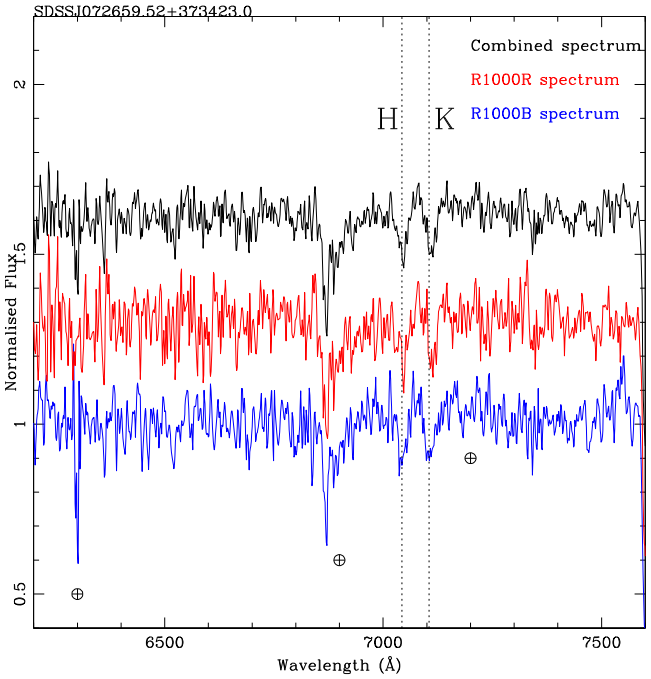

Figure 3. Close-up of the detected *H–K* band of Ca II in the spectrum of SDSS J072659.52+373423.0. Black line: joint R1000B+R1000R grism secured spectra. Red line: R1000R spectrum. Blue line: R1000B spectrum. See Table 2 for details of observations

(S/N = 50) for which identification is not obvious and could be potentially associated to Fe II intervening systems at $z \leqslant 1.45$. The continuum shape is more complex than usual BL Lac sources and cannot be described by a single power law in the optical region. We thus adopted a polynomial function to assess a fit of the continuum used to emphasize the faint spectral line.

SDSS J124700.72+442318.8: The only available spectroscopic redshift estimation of $z = 1.812$ comes from the SDSS Sky Survey and it is based on a narrow emission line at λ7857 Å ascribed to Mg II (2800 Å). We confirm the alleged emission lines in our spectrum (S/N = 60) at the same wavelength; however, the proposed interpretation as Mg II appears dubious. A more likely interpretation is emission from [O III] (5007 Å) at $z = 0.569$ on the basis of the very small FWHM ($\sim$300 km s^{-1}) and EW (2.30 Å). The target is also detected in the γ-ray band by the *Fermi* satellite (Acero et. al 2015).

SDSS J130925.52+430505.5: Plotkin et al. (2010) proposed a tentative redshift of $z = 1.154$ but no further indications of spectral features that sustain the measurements are reported. The target has been observed with the Keck telescope (equipped with LRIS) by Shaw et al. (2013), where they propose $z = 0.69$, interpreting the narrow emission line at $\sim$6298 Å as [O II] (3727 Å). In our higher S/N spectrum (S/N = 100), we confirm the presence of the [O II] (3727 Å) and we also clearly detect the emission line from [O III] (5007 Å) consistently at $z = 0.693$. In addition, we also detect an absorption feature that we ascribe to the Mg II system at $z = 0.690$ probably associated to the cool gaseous halo of the BLL. We remark also that this object belongs to the detected sources in *Fermi* 3LAT catalog (Acero et al. 2015).

SDSS J132802.09+112913.6: Plotkin et al. (2010), based on a single weak emission line detected at 7915 Å in the SDSS spectrum and interpreted as Mg II (2800 Å), proposed a tentative redshift $z = 1.827$. This value is not confirmed by our data (S/N = 30) since we clearly detect two prominent broad emission lines at 4409 Å (EW = 86 Å) ascribed to Mg II and [Ne V] consistently at $z = 0.580$. The feature at 7915 Å is indeed due to [O III] (5700 Å) (see Figure 1).

SDSS J144050.14+333350.2: From a single broad emission line heavily contaminated by a strong telluric band of O_2, a tentative redshift of $z = 1.774$ was suggested by Plotkin et al. (2010), interpreting it as Mg II. In addition to this feature, we also find further emission lines from C IV (1550 Å) and C III] (1909 Å) at redshift $z = 1.747$ that are slightly different from the previously suggested one. In fact, the broad feature identified by Plotkin et al. (2010) and detected also in our data corresponds to the transition of Mg II but with its blue wing strongly depressed by telluric lines. Finally, we also detect in our new data (S/N = 30) two intervening Mg II absorption systems at $z = 0.578$ and $z = 1.168$.

SDSS J145059.98+520111.7: The source was already discussed in Paiano et al. (2017b).

SDSS J152422.56+374034.1: On the basis of a tentative emission feature at 6200 Å Plotkin et al. (2010) proposed a redshift of $z = 1.219$. In our high quality spectrum (S/N = 40), we confirm the detection of this broad emission line at λ6204 Å ascribed to Mg II (2800 Å) and, moreover, an emission from C III] (1909 Å) at λ4235 at the same redshift.

SDSS J170108.89+395443.0: We firmly detect (S/N = 25) the emission line from Mg II (2800 Å) and C IV (1550 Å) at the redshift of $z = 1.895$. This confirms the tentative value proposed by Plotkin et al. (2010).

5. Conclusions

We obtained high quality optical spectra for 16 objects proposed to be BLLs at $z \geqslant 1$. For 5 of them, we disprove of the previous value of the redshift and find that they are indeed

at $z < 1$. For 8 other targets for which the redshift was based on only one spectral line, we are able to establish the value of z by detecting additional features. According to their spectral characteristics, we found that only 7 sources of the sample are bona fide BLLs, while the remaining 6 broad emission lines are revealed, indicating that they should be reclassified as Flat Spectrum Radio Quasars.

Finally, we comment on the remaining three sources where no emission lines are detected. In these targets only intervening absorption systems are apparent and we confirm the lower limit of $z \geqslant 3.367$, $\geqslant 3.140$, and $\geqslant 2.470$ for SDSS J120059.69+400913.1, SDSS J123132.37+013814.1, and SDSS J145059.98+520111.7 respectively. In these three spectra, no emission lines with EW > 1 Å are detected. This implies that if emission lines are present at redshift close to the highest z intervening system, their luminosity should be less than $\sim 10 \times 10^{42}$ erg s^{-1}. These values are much smaller than the typical distribution of emission line luminosity found for QSOs (Shen et al. 2011). This supports the fact that these targets are true BLL objects. They are the most distant BLLs ever detected and, remarkably, one of them (SDSS J145059.98+520111.7) is also a γ-ray emitter detected by *Fermi*-LAT (see Paiano et al. 2017a).

The determination of redshift of BLLs, especially in the distant universe, is both crucial and challenging. The availability of large telescopes with state-of-the-art instrumentation improved the outcome of this hunt, as demonstrated, e.g., in Shaw et al. (2013), Pita et al. (2014), Landoni et al. (2014, 2015b), and Paiano et al. (2017a, 2017b). Nevertheless, only the advent of Extremely Large Telescopes will greatly boost this line of research allowing us to study both extremely beamed sources and most distance targets where faintest spectral lines from host galaxies could be revealed thanks to the giant jump in terms of S/N (Landoni et al. 2014).

ORCID iDs

M. Landoni https://orcid.org/0000-0003-2204-8112
S. Paiano https://orcid.org/0000-0002-2239-3373
R. Falomo https://orcid.org/0000-0003-4137-6541
R. Scarpa https://orcid.org/0000-0001-9118-8739
A. Treves https://orcid.org/0000-0002-0653-6207

References

Acero, F., Ackermann, M., Ajello, M., et al. 2015, ApJS, 218, 23
Ajello, M., Romani, R. W., Gasparrini, D., et al. 2014, ApJ, 780, 73
Cepa, J., Aguiar-Gonzalez, M., Bland-Hawthorn, J., et al. 2003, Proc. SPIE, 4841, 1739
de Angelis, A., Galanti, G., & Roncadelli, M. 2011, PhRvD, 84, 105030
Falomo, R., Pian, E., & Treves, A. 2014, A&ARv, 22, 73
Franceschini, A., & Rodighiero, G. 2017, A&A, 603, A34
Landoni, M., Falomo, R., Treves, A., & Sbarufatti, B. 2014, A&A, 570, A126
Landoni, M., Falomo, R., Treves, A., Scarpa, R., & Reverte Payá, D. 2015a, AJ, 150, 181
Landoni, M., Massaro, F., Paggi, A., et al. 2015b, AJ, 149, 163
Liao, N.-H., Bai, J.-M., Wang, J.-G., et al. 2015, RAA, 15, 313
Madejski, G., & Sikora, M. 2016, ARA&A, 54, 725
Massaro, E., Maselli, A., Leto, C., et al. 2015a, Ap&SS, 357, 75
Massaro, F., D'Abrusco, R., Landoni, M., et al. 2015b, ApJS, 217, 2
Paiano, S., Falomo, R., Treves, A., & Scarpa, R. 2018, ApJL, 854, 32
Paiano, S., Landoni, M., Falomo, R., et al. 2017a, ApJ, 837, 144
Paiano, S., Landoni, M., Falomo, R., Scarpa, R., & Treves, A. 2016, MNRAS, 458, 2836
Paiano, S., Landoni, M., Falomo, R., Treves, A., & Scarpa, R. 2017b, ApJ, 844, 120
Pita, S., Goldoni, P., Boisson, C., et al. 2014, A&A, 565, A12
Plotkin, R. M., Anderson, S. F., Brandt, W. N., et al. 2010, AJ, 139, 390
Sandrinelli, A., Treves, A., Falomo, R., et al. 2013, AJ, 146, 163
Sbarufatti, B., Treves, A., Falomo, R., et al. 2006, AJ, 132, 1
Shaw, M. S., Romani, R. W., Cotter, G., et al. 2013, ApJ, 764, 135
Shen, Y., Richards, G. T., Strauss, M. A., et al. 2011, ApJS, 194, 45
Tavecchio, F., & Bonnoli, G. 2016, A&A, 585, A25